MRS Communications

https://doi.org/10.1557/s43579-021-00126-9

MRS Communications

Research Letter

The electronic states of ITO–MoS_2: Experiment and theory

Oscar A. López-Galán, and Manuel Ramos, Departamento de Física y Matemáticas, Instituto de Ingeniería y Tecnología, Universidad Autónoma de Ciudad Juárez., Avenida del Charro #450 N, Ciudad Juárez, Chihuahua, MX 32310, USA
John Nogan, Center for Integrated Nanotechnologies, Sandia National Laboratories, 1101 Eubank Bldg. SE, Albuquerque, NM 87110, USA
Alejandro Ávila-García, Departamento de Ingeniería Eléctrica, Sección de Electrónica del Estado Sólido, CINVESTAV del I.P.N., Av. Instituto Politécnico Nacional #2508, Sn. Pedro Zacatenco, Mexico City, MX 07360, USA
Torben Boll, Karlsruhe Nano Micro Facility (KNMF), Karlsruhe Institute of Technology (KIT), Hermann-von-Helmholtz-Platz 1, 76344 Eggenstein-Leopoldshafen, Germany
Martin Heilmaier, Institute for Applied Materials (IAM-WK), Karlsruhe Institute of Technology (KIT), Engelbert-Arnold-Str. 4, 76131 Karlsruhe, Germany

Address all correspondence to Torben Boll at **torben.boll@kit.edu**

(Received 20 July 2021; accepted 26 October 2021)

Abstract

We report a combination of experimental results with density functional theory (DFT) calculations to understand electronic structure of indium tin oxide and molybdenum disulfide (ITO–MoS_2) interface. Our results indicate ITO and MoS_2 conform an n-type Schottky barrier of c.a. – 1.0 eV due to orbital interactions; formation of an ohmic contact is caused by semiconducting and metal behavior of ITO as a function of crystal plane orientation. ITO introduces energy levels around the Fermi level in all interface models in the Γ-M-K-Γ path. The resulted Van der Waals interface and the values of Schottky barrier height enhance electron carrier injection.

Introduction

Layered two-dimensional materials have been highly attractive mainly for their usage to fabricate high-throughput low dimension electronic devices.[1,2] As encountered in the literature molybdenum disulfide (MoS_2), tungsten diselenide (WSe_2), graphene, and hexagonal boron nitride (hBN) were used as materials for nanotransistors,[3,4] phototransistors and photodetectors[5–7] due to high electron mobility and significant on/off current ratios that decreased power dissipation along with low cost and low dimensionality. In this regard, Schottky barrier height (SBH) and partial Fermi level pinning play a significant role for chemical contact between semiconductor–metal interfaces during operation.[8,9] Some of most used contact materials in semiconductor-based devices are gold, titanium, platinum, and nickel due to their low resistivity and chemical compatibility with semiconductors.

The seek for ohmic or low Schottky contact is a highly desirable properties of metal–semiconductor interfaces because it reduces energy losses and provides a linear dependency between current and applied voltage. An intense discussion regarding the presence of ohmic or Schottky contact in metal–semiconducting interfaces layered two-dimensional materials prevails in the scientific community. This has been highlighted by Das et al. who determined that metals promote *n*-type Schottky contacts when MoS_2 is combined with low work function metals like scandium (~ 3.5 eV) promoting a high electron carrier, thereby lowering the contact resistance.[10] Guo et al. used density functional theory (DFT) methods to predict metal-induced gap states with a combination of metals as top contacts on top of MoS_2, $MoSe_2$, $MoTe_2$, WS_2, WSe_2 and WTe_2 layers. They concluded that Schottky barrier height and pinning near Fermi level depend on the type of chemical bonding between the contact and the semiconductor material.[11] Li et al., by means of computational simulations, used titanium carbides Ti_2CY_2 (Y = F and OH) as contact materials with WSe_2 reporting that a Schottky contact is present with a barrier height of 0.40 eV.[12] By means of DFT Gao & Gupta reported that TiS_2 as contact material may possess both, ohmic and Schottky character with values of 0.3 eV to 1.35 eV, respectively.[13] By contrast, studies on the contact nature between ITO and MoS_2 are scarce in the literature despite the advantages that ITO offers as a transparent contact material.

Transparent ITO with a work function of ~ 4.4 eV and combined with MoS_2 was demonstrated to create a metallic–semiconducting interface.[14] This interface has been characterized by means of atom probe tomography (APT), which is a reconstruction technique to achieve physical information in three dimensions with near atomic resolution.[15] To investigate the electronic structure and electrical behavior, we present in here a series of DFT calculations on ITO–MoS_2 interfaces for both 2H and 3R MoS_2 polyforms and ITO based on experimentally obtained MoS_2 thin films deposited on ITO by radio frequency sputtering (RF sputtering). Our objective is to determine whether ITO provides a solid platform to achieve an either ohmic or low Schottky barrier contact when combining it with MoS_2 as a layered structure. If so, one could aim at using the material in micro and nanolayers for high efficiency solar cells and optoelectronic applications.

Methods and materials

MoS_2 and ITO sputtering

RF sputtering layers of Indium Tin Oxide (ITO) and Molybdenum disulfide (MoS_2) were deposited on commercial coupons for APT rendering using a Kurt J. Lesker PVD-75 equipment. Deposition time of ITO was set for 1800s with a chamber mixed with Argon (90%) and Oxygen (10%) at 20°C and 3 mT at 145 W. To achieve a homogenous layer of ITO a load of oxygen at 40% volume was introduced during ITO deposit. Once a layer of ITO is created the coupon was baked at 300°C for 20 min to achieve an ohmic contact material at atmospheric pressure using a 100 standard cm^3/min gas flow mixture of 3.8% H_2/Balance N_2; next, one layer of approximately 700 nm of MoS_2 was deposited in 3600 s as described in prior authors works.[16,17]

Atom probe tomography (APT)

The three-dimensional (3D) rendering of sulfur, molybdenum, indium, tin, and oxygen atoms was obtained by APT model Cameca® LEAP 4000X, equipped with a UV laser ($\lambda \sim 355$ nm). All APT measurements were taken at a set temperature of 50 K with an evaporation rate of 0.2 and a laser frequency of 100 kHz and laser beam at 20 pJ/V. Data rendering and three-dimensional (3D) reconstruction was completed with aid of Cameca IVAS© 3.6.14 package.

Scanning electron microscopy

Scanning electron microscopy was done via a Hitachi SU5500 equipped with an energy-dispersive X-ray unit and operated at 15 kV with 8A.

Computational methods

All proposed computational models were subjected to geometric optimization with CASTEP code[18] with a revised Perdew–Burke–Ernzerhof (RPBE) exchange–correlation functional as part of the generalized gradient approximation (GGA). Energy cutoff was set at 400 eV with a self-consistent field convergence criterion of 1×10^{-6} eV/atom and maximum displacement of 2×10^{-3} Å per atom. We employed a Brillouin zone mesh of $2 \times 2 \times 1$ k-point. For DFT calculations we used the 2H MoS_2 phase with lattice parameters of $a = b = 3.2$ Å, $c = 17.347$ Å and angles $\alpha = \beta = 90°$ and $\gamma = 120°$, 3R MoS_2 phase with lattice parameters of $a = b = 3.2$ Å, $c = 26.0$ Å and angles $\alpha = \beta = \gamma = 90°$, and ITO ($In_2Sn_2O_7$) unit cell with lattice parameters of $a = b = c = 7.3$ Å and $\alpha = \beta = \gamma = 60°$. The plane of contact along (002) for 2H and 3R MoS_2 phases was set using a surface of 2×2-cell and a thickness of c.a. 20 Å on top of ITO (222) and (400) surfaces, each with a crystal thickness of 10 Å, exposing oxygen surface. To ensure no periodic boundary conditions affect the geometrical optimizations, a vacuum space of 25 Å in z direction was placed for every interface model.

Results and discussion

Atom probe tomography and RF sputtering

The experimental fabrication of ITO and MoS_2 was completed by radio frequency sputtering, as described previously in Methods section aiming to determine whether ITO provides a platform to achieve a reliable contact with MoS_2 as a layered structure. An overview of the prepared layered structure (obtained by electron microscopy in scanning mode) can be seen in the Supplemental Material S1. Along with APT it was possible to determine a heterojunction interface between ITO and MoS_2 (see Fig. 1(a)) in agreement with Ramos et al.[16] APT analysis indicates negligible interaction between ITO and MoS_2 creating a well-defined interface. From this data, we can observe the approximate spatial distribution of atomic species of either ITO, corresponding to the lower part of model depicted in Fig. 1(a), and MoS_2, now corresponding to the upper part of the model of Fig. 1(a). In the 3D reconstruction, cyan balls represent molybdenum atoms, while yellow ones represent sulfur atoms; at the ITO side, red balls stand for oxygen species, black for tin, and purple for indium. With this, we were able to extract a representative portion of the sample (green rectangle in Fig. 1(a)) to model the interface used in the DFT calculations (Fig. 1(b)). MoS_2 deposited under the mentioned conditions tends to have needle-like crystallites nucleated along the <110> direction[17] as observed by scanning electron microscopy characterization (Fig. S2a). It is worth mention the fabrication methodology allows MoS_2 phase to remain encapsulated between ITO, avoiding degradation by exposure to air and moisture.[19] ITO is predicted to have preferential growth along [111] and [100] directions which signifies (222) and (400) planes as commonly observed on ITO layers deposited by RF sputtering technique.[20]

We estimated that the quality of the interface can be greatly improved whereby variation of the deposition parameters such as deposition time, RF power, and chamber conditions, i.e., as proposed by Samassekou et al.[21] In addition, achieving a well-defined interface can be attributed to the presence of an oxidized surface (ITO surface) in contact with the MoS_2 as previously stated by Muratore et al. where authors indicated that transition metal dichalcogenides growth are favored by oxygen-rich surfaces.[22]

The prediction of ITO preferential growth makes sense by computing the surface energy (γ) values of each surface considered in our DFT study compared to a hypothetical ITO surface. Surface energy (γ) calculations on the (222) and (400) ITO surfaces have lower values compared to the theoretical (440) ITO surface, as shown in Table S1, indicating why the latter have little evidence about its presence when ITO films are fabricated by RF sputtering.

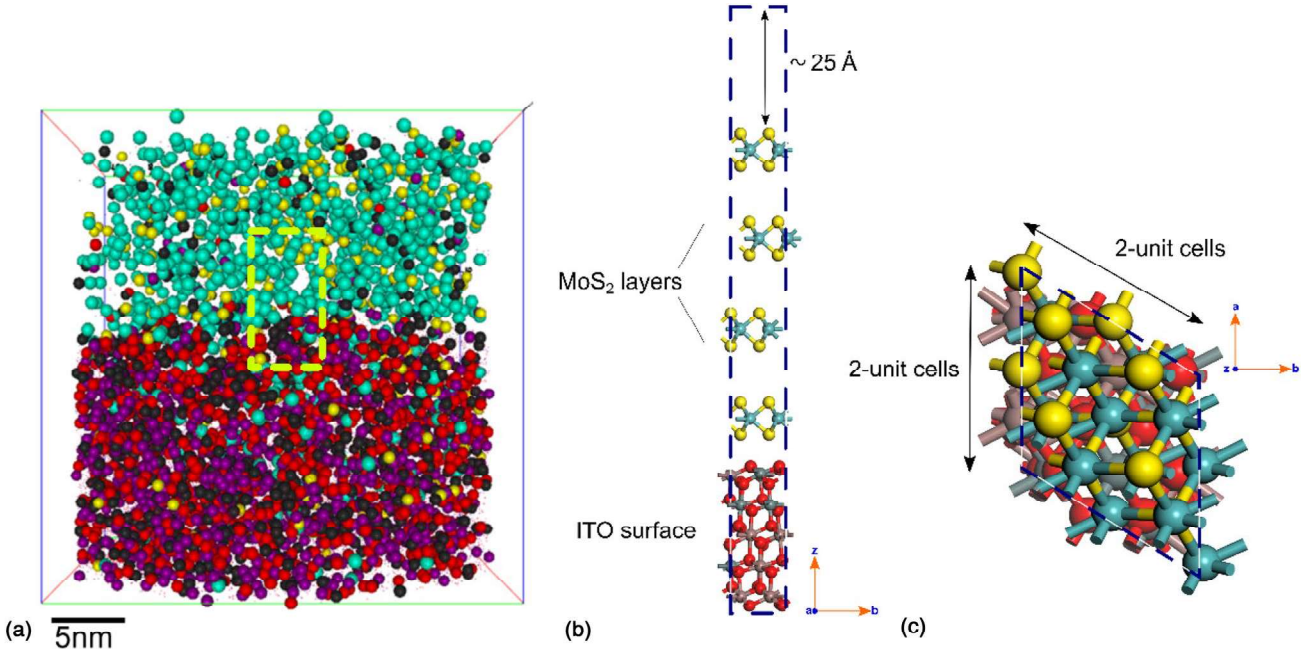

Figure 1. (a) Experimental atom probe tomography data (rendered) obtained from ITO–MoS_2 interfaces fabricated by RF sputtering technique. Green rectangle indicates the representative portion that we modeled in this work. (b) Schematic of our interface models (sideview) and (c) top view. In the *z* direction, each model differs depending on the MoS_2 phase and ITO surface direction. In our schematic, red balls indicate oxygen species, gray tin, brown indium, cyan molybdenum, and yellow sulfur.

Electronic structure of ITO–MoS_2 interfaces

Our theoretical model was built upon experimental information as obtained by atom probe tomography. In here we consider the (002)-plane of 2H and 3R MoS_2 to be in contact with (222) and (400) planes of ITO to create an interface (Fig. 1(b)). Our four proposed models are designated ITO_{222}-2HMoS_2, ITO_{222}-3RMoS_2, ITO_{400}-2HMoS_2 and ITO_{400}-3RMoS_2 in what follows. The aim of our DFT calculations was to understand electronic structure and behavior of the proposed interface models. We noticed that (222) ITO surface has a narrow bandgap of 0.133 eV and (400) ITO surface presents a metallic nature as presented in Fig. S4. This is in agreement with previous studies that indicate (400) planes enable a higher carrier injection -meaning free electrons- into the ITO in comparison with (222) planes.[20]

We found that ITO introduces several energy levels around the Fermi level in all our interface models seeing the band structure of the interface estimated for the Γ-M-K-Γ path (Fig. 2(a)); these additional energy levels leave an altered electronic structure compared to the band structure of isolated MoS_2 under bulk conditions (Fig. S4). The band structure results suggest that redistribution of molecular orbitals plays a major role in the electronic nature of the ITO–MoS_2 interfaces as hinted previously.[23] For the ITO_{222}-2HMoS_2 and ITO_{400}-3RMoS_2 structures the band structure resulted quite similar and without higher energy level insertion than ITO_{222}-3RMoS_2 and ITO_{400}-2HMoS_2 structures, which can be attributed a lower repulsion among orbitals and the spread of molecular orbitals without severe overlapping or hybridization. The insertion of energy states in the Γ-M-K-Γ path denotes the existence of a molecular orbital redistribution process, which eases the flow of charge through the material creating a contact with low resistivity.

From plots of the partial density of states, one deduces a low density of states near the Fermi level, which indicates two situations, first, that molybdenum atoms preserve their covalent binding behavior as in MoS_2 (Fig. 2(b)). This is contrary to what is found in metal–MoS_2 interfaces where a high density of *d* electrons appears in the vicinity of Fermi level[24] attributed to a disturbance of metallic *d* orbitals. Second, the similar distribution of the orbitals at the same region, indicates a low or partial hybridization, both at the top of the valence band and at the bottom of the conduction band. Moreover, by visualizing the individual distribution of orbitals from MoS_2 (s, p, and d orbitals) and ITO (s and d orbitals) and their partial density of states (Fig. 3), we see that ITO orbitals are those whose contribution are more pronounced just around de Fermi level, and thus, inserting energy states in the Γ-M-K-Γ path as stated previously. This process of s and p orbitals spreading through the bandgap happens without disturbance of molybdenum d orbitals and have a direct impact on the electronic distribution (and electrostatic potential) as discussed next.

Furthermore, the geometric optimized equilibrium distance (d_{eq}) at which MoS_2 and ITO create a Van der Waals interface is displayed in Table I. Hereby, d_{eq} is considered as minimum distance between ITO and MoS_2 for both 2H and 3R, which

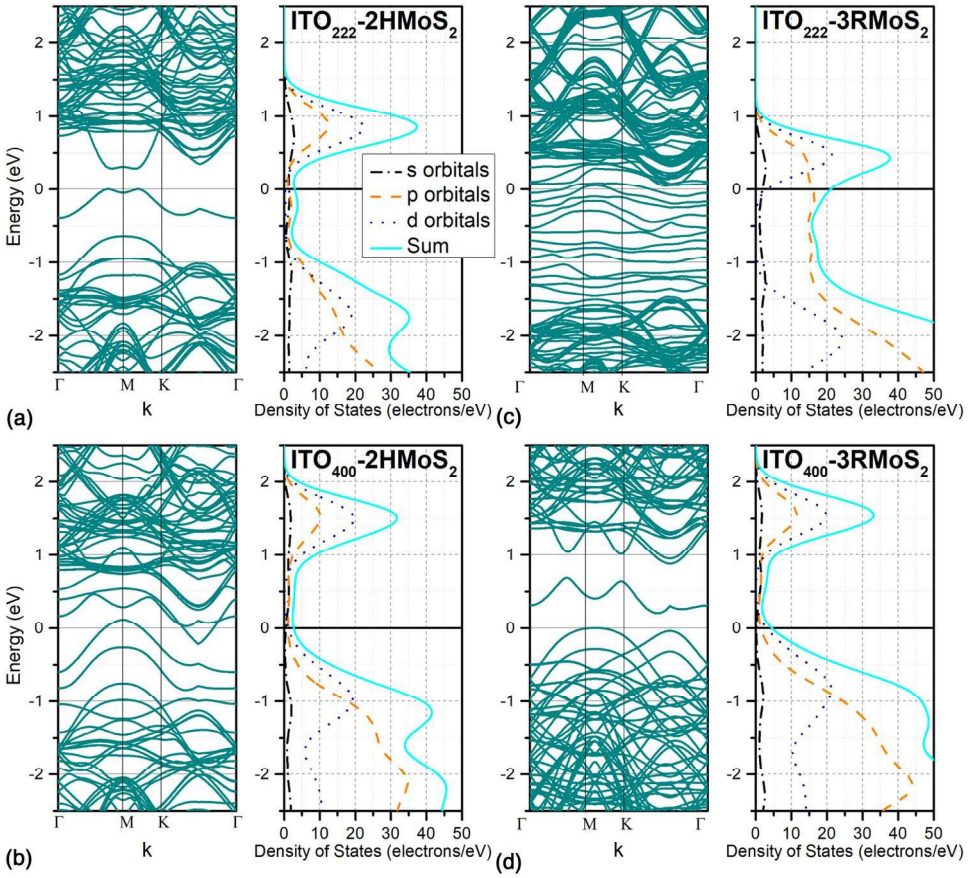

Figure 2. Band structure and partial density of states around the Fermi level estimation of ITO/MoS_2 models in the Γ-M-K-Γ path. The band intercrossing with the Fermi level (at the zero level) indicates semi-metallic behavior of the structure in all cases.

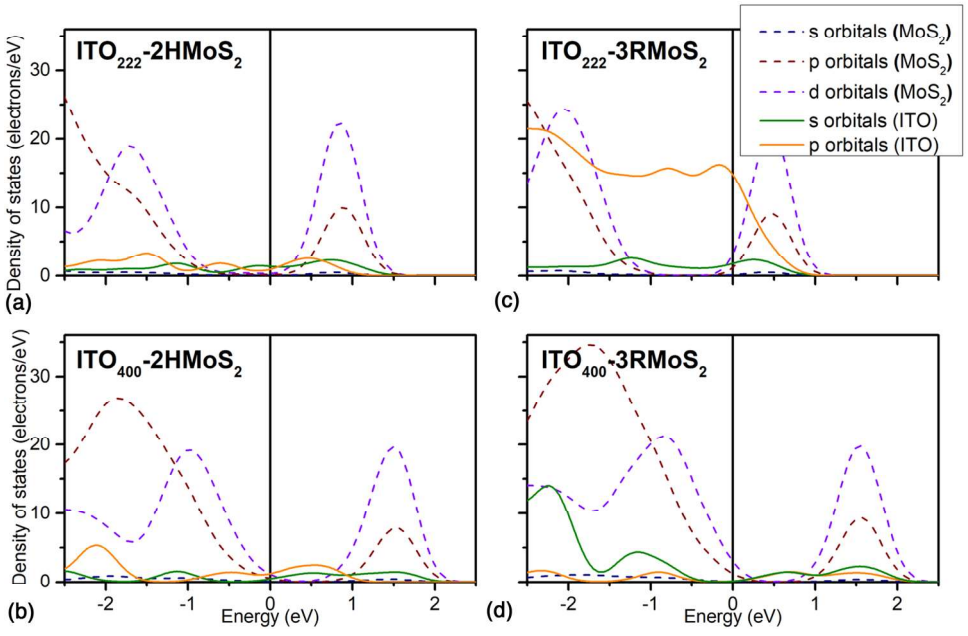

Figure 3. Contribution from s, p, and d orbitals from MoS_2 and ITO to the partial density of states for all four interface models. We observe that s and p orbitals from ITO contribute the more just in the vicinity of the Fermi level (located at 0 eV). Molybdenum d orbitals contribute to most of the valence and conduction band as reported previously.

Table I. Geometrical optimized equilibrium distance (d_{eq}) between ITO and MoS_2 to create a Van der Waals solid.

Surface/interface	d_{eq}/Å	W_{MoS2}	E_C	E_V	$W_{ITO-MoS2}$/eV	Δ_{ps}/eV	Φ_p/eV	Φ_n/eV
ITO_{222}-2HMoS_2	3.00	–	–	–	3.75	− 0.002	3.45	− 1.65
ITO_{222}–3RMoS_2	3.10	–	–	–	3.83	− 0.077	3.45	− 1.65
ITO_{400}–2HMoS_2	3.14	–	–	–	3.20	1.395	3.00	− 1.19
ITO_{400}–3RMoS_2	3.50	–	–	–	4.31	1.277	2.96	− 1.15
2H MoS_2	–	5.6	5.4	7.2	–	–	–	–
3R MoS_2	–	5.66	5.46	7.27	–	–	–	–

The estimated $W_{ITO-MoS2}$, calculated Δ_{ps}, *p*-type Schottky barrier (Φ_p) and *n*-type Schottky barrier (Φ_n) for each interface. Δ_{ps} calculation include a correction of W_{ITO} fitted onto MoS_2 lattice parameters as discussed in Supplemental Material S2. Work function of 2H and 3R MoS_2 and position of the conduction (E_C) and valence band (E_V).

is chemically detached from ITO to form a Van der Waals interface -typical contact distances between 2.8 and 4.0 Å, and approximately 3.2 Å for graphite interlayer distance. We calculated that d_{eq} ranges from 3.0 to 3.5 Å (Fig. 4(a)). Despite these relatively large values, the nature of the electronic configuration of ITO and MoS_2 lead us to expect an interaction between s, p, and d orbitals on ITO–MoS_2 interfaces, implying the electronic structure compatibility toward usage on fabrication of microelectronic devices, mainly as transparent-semiconductor nanolayers for solar cells applications as demonstrated before.[14]

Schottky barrier formation and band alignment estimation at the MoS_2/ITO interface

The Schottky–Mott theory states that having an ohmic contact for an n-type semiconductor requires a material, typically a metal, whose work function is comparably close to the electron affinity of the semiconductor (χ_s). Dipole formation in the ITO–MoS_2 interface shows a dependence on the ITO surface as displayed in Table I (see details in Supplementary Material S3). The *p*-type Schottky barrier height in our model is defined as[25]

$$\Phi_p = E_V - W_{ITO} + \Delta_{ps} \quad (1)$$

where the additional term Δ_{ps} is included to consider the dipole formation at the interface. E_V and W_{ITO} are the position of the valence band and the work function of the clean ITO surface (see Supplementary Material S2), respectively.

The *n*-type SBH is defined as

$$\Phi_n = E_g - \Phi_p \quad (2)$$

where E_g is the bandgap of MoS_2, calculated with respect to the vacuum level.

The p- and n-type Schottky barrier height estimations are summarized in Table I for each ITO–MoS_2 interface considered. Remarkably, all our interface models present positive and negative values of Φ_p and Φ_n, respectively, indicating the formation of ohmic contacts in all cases, which are larger to those reported in other metal-transition metal dichalcogenides interfaces.[12,13] The calculation of positive and negative values of Φ_p and Φ_n, respectively, suggest a high carrier injection into the interface expecting similar carrier injection as in MoS_2 sandwiched between layers of ITO and Cu_2O.[26] All p- and n-type Schottky barrier height values remain close to each other, suggesting a dependence on MoS_2 phase.

From the estimation of band alignment, a band bending downwards is expected because of the negative values of Φ_n (Fig. S6). This band bending then induces an electron accumulation region in the MoS_2 near the interface. Electron accumulation at the MoS_2 side would induce a positive charge at the ITO side, thus, one would not expect significant energy losses and a high injection of charge carriers throughout the interface, creating a contact of ohmic nature; a linear dependency between current and applied voltage is expected.

We assume that two main factors are responsible for these particularly values of Schottky barrier height: carrier concentration and work function modification. As described in Supplemental Material S4, one notes that the estimated contact resistance of our interface models (R_c) decays strongly around 1 Ωcm^2 (considering an intermediate carrier concentration in MoS_2) indicating an ohmic contact behavior and a field emission mechanism dominance.[27] As a consequence, an interaction either between ITO and MoS_2 orbitals or within each material has to occur at least to some degree,[24] similar to other interface scenarios with involvement of MoS_2.[28]

In here, we neglect the chemical nature of the work function decrease due to the lack of chemical bonding between ITO and MoS_2 because it is considered a Van der Waals heterojunction. Then, the effect must be attributed to the distribution of orbitals of each material. The estimated partial density of states as shown in Figs. 2 and 3, indicates a low degree of hybridization between ITO and MoS_2 exemplified by the low density of states around the Fermi level and the same curves' behavior; in addition, electron density difference plots of our four interface models are indicating a small interaction between ITO, Mo, and S orbitals (Fig. 4). However, this interaction is strong enough to achieve a conduction channel but not strong enough to disturb the MoS_2 electronic structure and the small insertion of states at the bandgap (Fig. 3) is mainly caused by orbitals from sulfur, oxygen, indium, and tin atoms.

The electrostatic potential (*C*) plotted parallel to the *z* direction of the surfaces shows a significant alteration of the

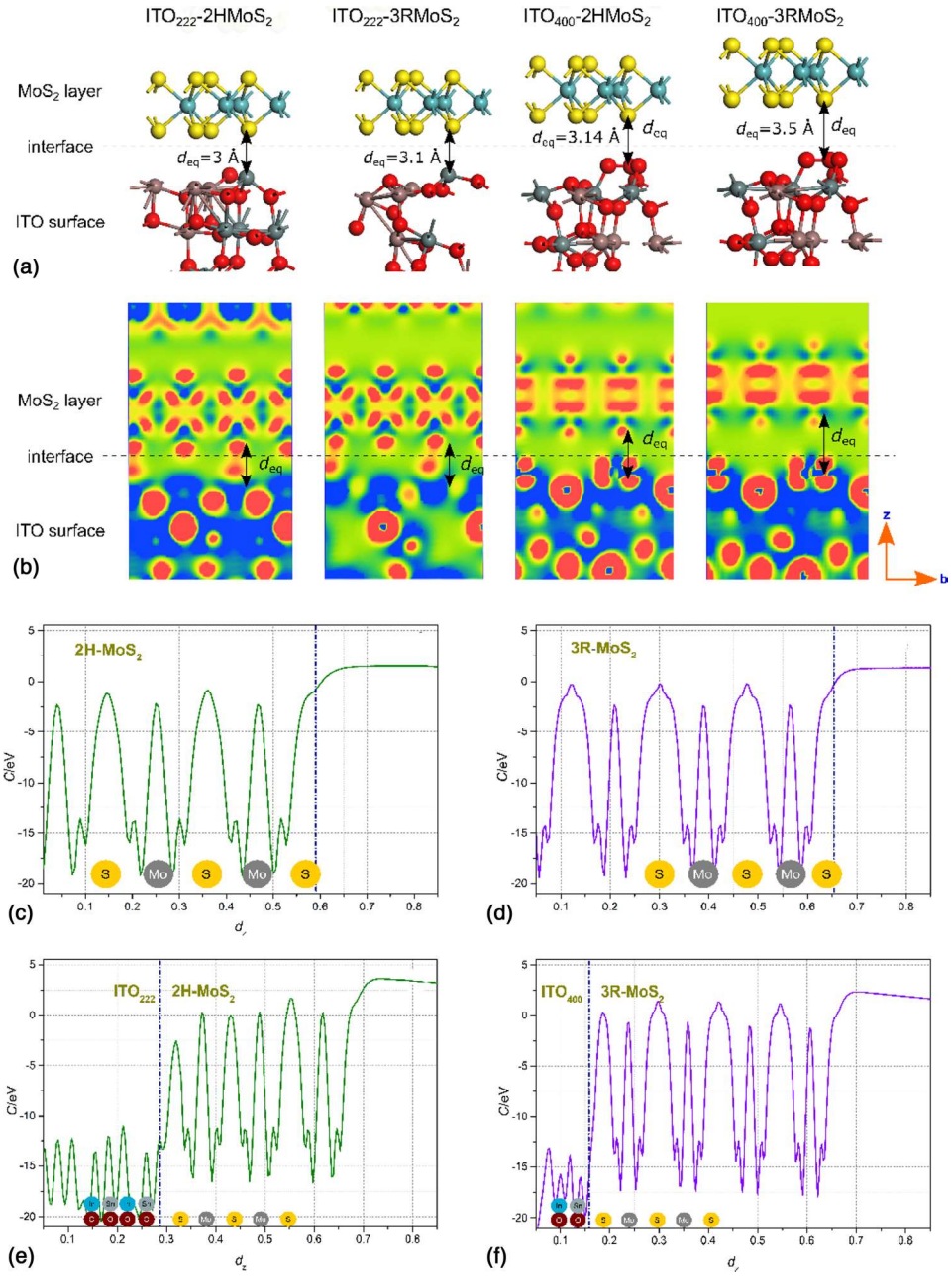

Figure 4. (a) Geometric optimization series and (b) electron density difference (EDD) profiles obtained. The EDD plots indicate an electronic migration occurring between ions, and blue zones indicate depletion of electrons, red zones indicate electron enrichment, finally green zones indicate neutralized charge. The d_{eq} corresponds to equilibrium distance between ITO and MoS_2 contact. The yellow color balls correspond to sulfur atoms and blue represent molybdenum atoms for MoS_2 proposed model. The red, brow, and gray balls indicate oxygen, tin, and indium, respectively. (c) Electrostatic potential (C) for the isolated $2HMoS_2$ surface, (d) isolated $3RMoS_2$, (e) $ITO_{222}/2HMoS_2$ and (f) $ITO_{400}/3RMoS_2$ interfaces with respect to the fractional distance in the z direction (d_z). Blue dashed line indicates the surface and the interface location for the $2HMoS_2$, $3RMoS_2$ surface and the $ITO_{222}/2HMoS_2$ and $ITO_{400}/3RMoS_2$ interface.

potential after the formation of the interface at the MoS_2 side (Fig. 4(c)–(f)). Such change results from repulsion between the uppermost electrons 2s and 2p, belonging to oxygen, and the bottom electrons from the sulfur, also 2s and 2p. This then suggest that these orbitals hybridize inside each material changing the electrostatic of the material and hence, the work function on each side. Moreover, the bulk part of ITO successfully acts as an electron reservoir allowing the repulsed electrons to reallocate the 2s with point symmetry a_{1g} and 2p with point symmetry t_{1u} orbitals from oxygen without further hybridization with MoS_2[29] and without disturbance of metallic molybdenum *d* orbitals. These delocalized electrons explain

the high carrier injection in such interfaces and the creation of an ohmic contact.

Lack of hybridization of surface electronic orbitals between ITO and MoS_2 can be understood recalling the preferred octahedral coordination in MoS_2 and ITO. This is exemplified in Figs. S7a and S7b as schematic molecular orbitals of metal oxides, resembling what happens in indium tin oxide, and MoS_2, respectively. In the first case, e_g point symmetry metal orbitals corresponding to the 4d level (equivalent to the $d_{x^2-y^2}$ and d_{z^2} orbitals) are aligned with the 2p oxygen orbitals resulting in strong overlap and hybridization of orbitals. In second case, triple degenerated t_{2g} orbitals (d_{xy}, d_{yz} and d_{xz} orbitals) yield a small overlap with the 2p orbitals of oxygen or sulfur because of misalignment between orbitals leading only to weak π bonds.

Similarly, in the MoS_2 model (Fig. S7b), 4d molybdenum orbitals aligned with the 3p sulfur orbitals results in strong hybridization having MoS_2 characteristic metallic edges.[30] However, the lack of available t_{1u} orbitals (p orbitals) allows a_{1g} (s orbitals) to extend, modifying the distance between the unoccupied and occupied molecular orbitals, leading to the formation of the bandgap (E_g). Without hybridization, overlap between same symmetry orbitals would leads to the formation of a continuum of levels and the loss of E_g.

Conclusions

Our electronic structure calculations, based on density functional theory and on experimental information from atom probe tomography of RF sputtered ITO–MoS_2 interface, indicates that ohmic contact are present within MoS_2 and ITO architecture. The calculations of contact planes of ITO (222) and (400) coupled with 2H and 3R MoS_2 implies formation of ohmic contacts in all cases with remarkably negative values of n-type Schottky barrier height (Φ_n) of around − 1.6 eV for 2H and − 1.2 eV for 3R MoS_2 and a computed contact resistance of about 1 Ωcm^2. We attributed this behavior to the non-disturbance of metallic molybdenum *d* orbitals. Finally, the results from this work provides important insights about ITO and MoS_2 materials towards development of nanoscale device fabrication for next generation of high efficiency photovoltaic devices and optoelectronic applications.

Acknowledgments

This work was supported by Instituto de Ingeniería y Tecnología of Universidad Autónoma de Cd. Juárez (UACJ) and Programa de Fortalecimiento a la Calidad Educativa (PFCE) 2016-2017 of División Multidisciplinaria of Ciudad Universitaria for licensing BIOVIA-Materials Studio© and the use of high-performance computing facilities. Principal author thank Consejo Nacional de Ciencia y Tecnología (CONACyT) of Mexico for graduate scholarship #735528. To the Karlsruhe Nano and Micro Facility of Karlsruhe Institute of Technology in Germany for usage of atom probe tomograph and electron microscopy equipment. Authors appreciate the availability of the Center for Integrated Nanotechnologies, an Office of Science User Facility operated for the U.S. Department of Energy (DOE) Office of Science, for the usage of PVD equipment.

Funding

Open Access funding enabled and organized by Projekt DEAL. This work was funded by Instituto de Ingeniería y Tecnología of Universidad Autónoma de Cd. Juárez (UACJ) and Programa de Fortalecimiento a la Calidad Educativa (PFCE) 2016–2017 of División Multidisciplinaria of Ciudad Universitaria. Part of this work was performed at the Center for Integrated Nanotechnologies, an Office of Science User Facility operated for the U.S. Department of Energy (DOE) Office of Science. Sandia National Laboratories is a multi-program laboratory managed and operated by Sandia Corporation, a fully owned subsidiary of Lockheed Martin Corporation, for the U.S. Department of Energy's National Nuclear Security Administration under contract DE-AC04-94AL85000.

Availability of data and material

The datasets generated during and/or analyzed during the current study are available from the corresponding author on reasonable request.

Declarations

Conflict of interest

All authors declare that they have neither financial nor personal interests that could affect the manuscript and results.

Supplementary Information

The online version contains supplementary material available at https://doi.org/10.1557/s43579-021-00126-9.

References

1. S.J. McDonnell, R.M. Wallace, Atomically-thin layered films for device applications based upon 2D TMDC materials. Thin Solid Films **616**, 482–501 (2016). https://doi.org/10.1016/j.tsf.2016.08.068
2. N. Briggs et al., A roadmap for electronic grade 2D materials. 2D Mater. **6**(2), 022001 (2019). https://doi.org/10.1088/2053-1583/aaf836
3. B. Sirota, N. Glavin, A.A. Voevodin, Room temperature magnetron sputtering and laser annealing of ultrathin MoS_2 for flexible transistors. Vacuum **160**, 133–138 (2019). https://doi.org/10.1016/j.vacuum.2018.10.077
4. B. Radisavljevic, A. Radenovic, J. Brivio, V. Giacometti, A. Kis, Single-layer MoS_2 transistors. Nat. Nanotechnol. **6**(3), 147–150 (2011). https://doi.org/10.1038/nnano.2010.279
5. H. Henck et al., Electrolytic phototransistor based on graphene-MoS_2 van der Waals p-n heterojunction with tunable photoresponse. Appl. Phys. Lett. **109**(11), 113103 (2016). https://doi.org/10.1063/1.4962551
6. U.N. Noumbé et al., Ionic Glass-Gated 2D Material-Based Phototransistor: $MoSe_2$ over LaF_3 as Case Study. Adv. Funct. Mater. **29**(33), 1902723 (2019). https://doi.org/10.1002/adfm.201902723
7. D. Kufer, G. Konstantatos, Photo-FETs: phototransistors enabled by 2D and 0D nanomaterials. ACS Photon. **3**(12), 2197–2210 (2016). https://doi.org/10.1021/acsphotonics.6b00391
8. K.M. Freedy, S.J. McDonnell, Contacts for molybdenum disulfide: interface chemistry and thermal stability. Materials **13**(3), 693 (2020). https://doi.org/10.3390/ma13030693
9. A. Allain, J. Kang, K. Banerjee, A. Kis, Electrical contacts to two-dimensional semiconductors. Nat. Mater. **14**(12), 1195–1205 (2015). https://doi.org/10.1038/nmat4452
10. S. Das, H.-Y. Chen, A.V. Penumatcha, J. Appenzeller, High performance multilayer MoS_2 transistors with scandium contacts. Nano Lett. **13**(1), 100–105 (2013). https://doi.org/10.1021/nl303583v
11. Y. Guo, J. Robertson, Schottky barrier heights and band alignments in transition metal dichalcogenides. Microelectron. Eng. **147**, 184–187 (2015). https://doi.org/10.1016/j.mee.2015.04.069
12. Q. Li et al., Ohmic contacts between monolayer WSe_2 and two-dimensional titanium carbides. Carbon **135**, 125–133 (2018). https://doi.org/10.1016/j.carbon.2018.04.043
13. J. Gao, M. Gupta, Titanium disulfide as Schottky/ohmic contact for monolayer molybdenum disulfide. Npj 2D Mater. Appl. **4**(1), 26 (2020). https://doi.org/10.1038/s41699-020-00161-5
14. M.A.R. Murillo, J.J. Nogan, R.C.A. Lazaro, C.A.R. González, M.O. Diaz, J.L. Enriquez-Carrejo, J.M. Jr. Garcia. Organic-semiconducting hybrid solar cell, US10727428B1. https://patents.google.com/patent/US10727428B1/en
15. T.F. Kelly, D.J. Larson, Atom probe tomography 2012. Annu. Rev. Mater. Res. **42**(1), 1–31 (2012). https://doi.org/10.1146/annurev-matsci-070511-155007
16. M. Ramos et al., Study of indium tin oxide–MoS_2 interface by atom probe tomography. MRS Commun. **9**(4), 1261–1266 (2019). https://doi.org/10.1557/mrc.2019.150
17. M. Ramos et al., Mechanical properties of RF-sputtering MoS_2 thin films. Surf. Topogr. Metrol. Prop. **5**(2), 025003 (2017). https://doi.org/10.1088/2051-672X/aa7421
18. S.J. Clark et al., First principles methods using CASTEP. Z. Für Krist.-Cryst Mater. **220**, 567–570 (2005)
19. P. Budania et al., Long-term stability of mechanically exfoliated MoS_2 flakes. MRS Commun. **7**(4), 813–818 (2017). https://doi.org/10.1557/mrc.2017.105
20. L. Dong et al., Preparation of indium tin oxide (ITO) thin film with (400) preferred orientation by sol–gel spin coating method. J. Mater. Sci. Mater. Electron. **30**(8), 8047–8054 (2019). https://doi.org/10.1007/s10854-019-01126-1
21. H. Samassekou, A. Alkabsh, K. Stiwinter, A. Khatri, D. Mazumdar, Atomic-level insights through spectroscopic and transport measurements into the large-area synthesis of MoS_2 thin films. MRS Commun. **8**(3), 1328–1334 (2018). https://doi.org/10.1557/mrc.2018.167
22. C. Muratore, A.A. Voevodin, N.R. Glavin, Physical vapor deposition of 2D Van der Waals materials: a review. Thin Solid Films **688**, 137500 (2019). https://doi.org/10.1016/j.tsf.2019.137500
23. S. Dam, A. Thakur, S. Hussain, Valence band studies of MoS_2 thin films synthesised by electrodeposition method. Mater. Today Proc. (2020). https://doi.org/10.1016/j.matpr.2020.03.722
24. C. Gong, L. Colombo, R.M. Wallace, K. Cho, The unusual mechanism of partial Fermi level pinning at metal–MoS_2 interfaces. Nano Lett. **14**(4), 1714–1720 (2014). https://doi.org/10.1021/nl403465v
25. M. Bokdam, G. Brocks, M.I. Katsnelson, P.J. Kelly, Schottky barriers at hexagonal boron nitride/metal interfaces: a first-principles study. Phys. Rev. B **90**(8), 085415 (2014). https://doi.org/10.1103/PhysRevB.90.085415
26. S. Kallatt, S. Nair, K. Majumdar, Asymmetrically encapsulated vertical ITO/MoS_2/Cu_2O photodetector with ultrahigh sensitivity. Small **14**(3), 1702066 (2018). https://doi.org/10.1002/smll.201702066
27. G. Greco, F. Iucolano, F. Roccaforte, Ohmic contacts to gallium nitride materials. Appl. Surf. Sci. **383**, 324–345 (2016). https://doi.org/10.1016/j.apsusc.2016.04.016
28. L. Rao, H. Liu, W. Shao, X. Xing, Y. Zhou, Q. Yang, Adhesion property and bonding characteristic between TiN and 2D-MoS_2: a first-principles study. J. Mater. Res. (2021). https://doi.org/10.1557/s43578-021-00197-3
29. C. Gong et al., Metal–graphene–metal sandwich contacts for enhanced interface bonding and work function control. ACS Nano **6**(6), 5381–5387 (2012). https://doi.org/10.1021/nn301241p
30. M.A. Ramos, R. Chianelli, J.L. Enriquez-Carrejo, G.A. Gonzalez, G. Berhault, Metallic states by angular dependence in 2H-MoS_2 slabs. Comput. Mater. Sci. **84**, 18–22 (2014). https://doi.org/10.1016/j.commatsci.2013.11.038